www.sciencemag.org/cgi/content/full/341/6149/1012/DC1

# Supplementary Material for

## Crystal Structure of MraY, an Essential Membrane Enzyme for Bacterial Cell Wall Synthesis

Ben C. Chung, Jinshi Zhao, Robert A. Gillespie, Do-Yeon Kwon, Ziqiang Guan, Jiyong Hong, Pei Zhou, Seok-Yong Lee*

*Corresponding author. E-mail: sylee@biochem.duke.edu

Published 30 August 2013, *Science* **341**, 1012 (2013)
DOI: 10.1126/science.1236501

**This PDF file includes:**

Materials and Methods

Expression and purification

To identify an optimal candidate for crystallization, we screened MraYs from 19 different species. We found that MraY from *Aquifex aeolicus* ($MraY_{AA}$) was most suitable for structural and functional studies judging from its biochemical stability. The codon-optimized gene corresponding to $MraY_{AA}$ was synthesized, and protein was expressed in C41 (DE3) cells as a fusion with a decahistidine-maltose binding protein (His-MBP) followed by a PreScission protease site between the enzyme and His-MBP segments. The fusion protein was extracted from membranes by dodecyl-maltoside and purified using a $Co^{2+}$-affinity column. The His-MBP was then removed from the enzyme by PreScission protease cleavage, and $MraY_{AA}$ was purified to homogeneity using size exclusion chromatography (SEC). SeMet-substituted MraY was obtained using auto-induction as reported (*20*). Methods of purification and crystallization of SeMet-$MraY_{AA}$ were similar to those of $MraY_{AA}$.

Crystallization, phasing, and model building

Extensive crystallization attempts were performed using in-house crystallization screen solutions. Crystals from most conditions diffracted poorly (>20 Å), but crystals grown in the presence of $Mg^{2+}$ showed promise with anisotropic diffraction (two directions 4.5 Å and one direction ~7.5 Å). The optimized crystals grew in the following conditions: 8-10 mg/mL $MraY_{AA}$ in a buffer containing 150 mM sodium chloride, 20 mM Tris pH 8.0, 5 mM DM, and 2 mM DTT was mixed with a crystallization solution containing 20-120 mM magnesium acetate, 9 mM nickel chloride, 50 mM sodium cacodylate pH 5.6, and 45% PEG400. Crystals appeared within a few days and were fully grown within 7 to 14 days at 17 $^{o}$C. SeMet-substituted MraY crystals were grown in similar conditions with slightly lower protein concentrations. Initial SAD phasing was obtained from a SeMet-MraY crystal that diffracted to 3.9 Å using the ID 24-C beam line at the Advanced Photon Source. SHELX was used to identify Se sites (*21*), and Phenix was used to calculate phases using the Se substructures (*22*). There are two $MraY_{AA}$ molecules in the asymmetric unit, which allowed us to perform non-crystallographic symmetry averaging as well as solvent flattening at 3.9 Å using RESOLVE from the Phenix package (*22*). At this stage, electron density for many transmembrane helices was discernible and allowed us to place idealized poly-Ala helical fragments manually. With this partial model, we calculated phasing from a combination of molecular replacement and single anomalous dispersion (MR-SAD), which improved the phases significantly. The 3.3 Å native data was subjected to ellipsoidal truncation and anisotropic scaling before phase extension and refinement using the UCLA diffraction anisotropy server (*23*). All the Se positions were identified by an anomalous difference Fourier map, which guided model building. To further help model building, a mutant SeMet crystal (L105M) was grown and the introduced methionine was identified by an anomalous difference Fourier map. The structural model of MraY was built both manually and using the automatic model-building software AutoBuild from Phenix (*22*). The final model was refined to $R_{work}/R_{free}$ = 22.3/26.5 % with good geometry and contains amino acids 14 – 48, 70 –357 for one

protomer (chain A) and 14 – 48, 70 –121, 126–311, 334–357 for the other protomer (chain B), two $Mg^{2+}$ ions, and two $Ni^{2+}$ ions (table S1 and S2).

Synthesis of capuramycin

Capuramycin was synthesized with modifications to the procedure described by Kurosu *et al* (*24*).

TLC-based translocase assay

The translocase assay, typically 15 μL in volume, was performed *in vitro* at 30 °C in an assay buffer consisting of 100 mM Tris-HCl pH 7.5, 500 mM sodium chloride, 0.25% w/v decylmaltoside, 10 mM $MgCl_2$, 1.1 mM undecaprenyl phosphate, 250 μM (1000 cpm/μL) UDP-MurNAc-[$^{14}$C]-pentapeptide. Both radiolabeled and non-labeled UDP-MurNAc-pentapeptide were purchased from the synthetic facility at the University of Warwick (*25, 26*). $C_{55}$-P was purchased from Larodan. The reaction was initiated by the addition of enzyme to a final concentration of 100 μg/ml. At the appropriate time point, the reaction was quenched by spotting a 3-μl aliquot on a silica gel 60 TLC plate. The reaction substrates and products were separated by TLC using a mobile phase with isopropanol : ammonium hydroxide : water (6:3:1, v/v), as previously described (*13*). After developing, the plates were dried under a stream of cold air and analyzed via PhosphorImager. The observed $R_f$ values for the substrate UDP-MurNAc-pentapeptide (~0.19) and product Lipid I (~0.50) are comparable to previously published results (0.25 and 0.58 respectively)(*13*). The results for the mutants are based on substrate conversion after 20 minutes of reaction at 30 $^{o}$C. The protein concentrations of the wild type and mutant enzymes were determined by UV molar absorptivity. The capuramycin inhibition assay was performed with the same procedure, except that varying concentrations of capuramycin were pre-incubated with $MraY_{AA}$ for 20 minutes at 30 $^{o}$C, and the capuramycin-$MraY_{AA}$ mixture was added to the reaction buffer to initiate the reaction. For metal dependence experiments, apo-$MraY_{AA}$ was formed by incubating purified $MraY_{AA}$ with 2 mM EDTA for 30 minutes on ice. Apo-$MraY_{AA}$ was then diluted 5-fold into purification buffer containing metals as specified and incubated for an additional 30 minutes on ice. The reaction was initiated by adding the metal/$MraY_{AA}$ mixture to the same reaction buffer with metal at the indicated concentrations. The results for the capuramycin and the metal-dependence assays were based on substrate conversion from 10 to 30 min.

Cross-linking experiments

We performed cross-linking studies of $MraY_{AA}$ both in detergent micelles and cell membranes as described (*27*). Purified $MraY_{AA}$ in decylmaltoside was subjected to cross-linking using the membrane-permeable cross-linking reagent disuccinimidyl suberate (DSS) at various concentrations at room temperature. The reaction was quenched after 25 min with the addition of 100 mM Tris buffer and then subjected to gel electrophoresis. The oligomeric status of $MraY_{AA}$ was identified by Coomassie staining. As for the structure-based disulfide bridge experiment, *E. coli* cells membranes were isolated and

subjected to cross-linking using the membrane-permeable oxidant copper phenanthroline (200 μM) at room temperature. The reaction was quenched after 25 min with the addition of 18 mM N-ethylmaleimide (NEM) and 45 mM EDTA. Protein loading buffer containing SDS was subsequently added to the membranes to a final SDS concentration of 2% (w/w) for solubilization. The oligomeric status of $MraY_{AA}$ was identified by Western blot using anti-His antibodies.

Anomalous scattering experiments

All the data for anomalous scattering studies were collected at the BM22 beamline at the Advanced Photon Source. To identify the position of $Mg^{2+}$, we prepared two types of crystals. The best-diffracting $MraY_{AA}$ crystal form requires both $Mg^{2+}$ and $Ni^{2+}$ for successful growth. Co-crystallization of MraY crystals with $Mn^{2+}$ and $Ni^{2+}$ was not successful; therefore we replaced $Mg^{2+}$ in the crystals with $Mn^{2+}$ by soaking the native crystal in a $Mn^{2+}$-containing mother liquor. To replace $Mg^{2+}$ with $Mn^{2+}$, about half of the drop solution was removed and 2 μL of crystallization solution containing 50 mM $Mn^{2+}$ was added and equilibrated for 10 min, after which the process was repeated two more times. We also grew crystals with only $Mn^{2+}$. To grow crystals in the presence of $Mn^{2+}$ only (without $Mg^{2+}$ and $Ni^{2+}$), crystals were grown with 70 mM $Mn^{2+}$. The crystals possess very similar unit cell dimensions (a=97.3, b=100.46, c=141.63) and very similar crystal packing as the native crystal, but a different space group ($C222_1$) from the native crystal ($P2_12_12_1$). The change of the space group in the absence of $Ni^{2+}$ was also observed with crystals grown in the presence of only $Mg^{2+}$. The $Mn^{2+}$-only crystals diffracted at a lower resolution (5.2 Å), but the $Mn^{2+}$ anomalous signal from this crystal was stronger (~6 σ). The $Mn^{2+}$-soaked crystal and the crystal grown in the presence of $Mn^{2+}$ diffracted X-rays to 5.2 Å and 5.7 Å, respectively. A long wavelength (1.50-1.55 Å) was utilized to maximize the anomalous scattering power. Anomalous difference Fourier maps were calculated using the model phases without any metals.

To identify the ions in loop E, we calculated an anomalous difference Fourier map using the 3.3-Å native data that was collected at a short wave length (0.975 Å) from the crystal grown in the presence of $Mg^{2+}$ and $Ni^{2+}$.

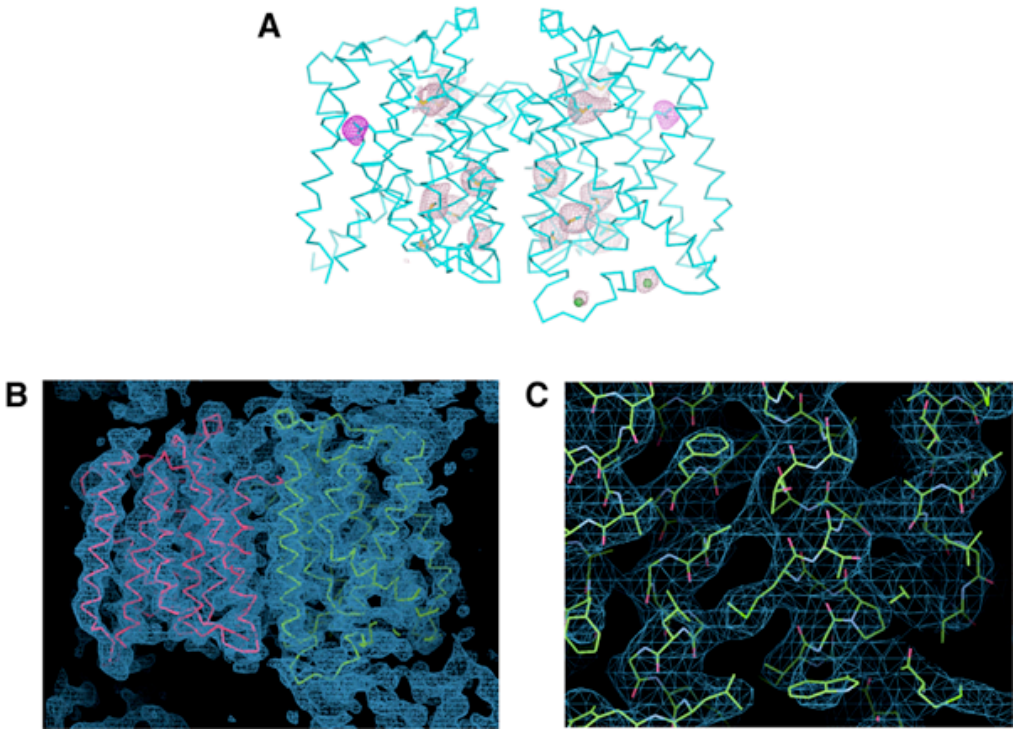


**Fig. S1**

Experimental phases. (**A**) Anomalous difference Fourier density peaks for selenium and $Ni^{2+}$ ions (green spheres) are shown in salmon mesh (2.5σ). The map was calculated using the SAD phasing from the SeMet data using 40 Å to 3.9 Å. The final model is shown in Cα representation with all 14 methionines shown in stick representation. The anomalous difference Fourier density peaks for the introduced mutation (L105M) are shown in pink mesh, contoured at 3σ. (**B**) The phase-extended and non-crystallographic two-fold averaged electron density map calculated from the 3.9 Å Se-SAD phases and the amplitudes of the 3.3-Å native data. The amplitudes of the native data were subjected to anisotropic scaling prior to phase extension. The final model is shown in Cα representation with each protomer colored separately. (**C**) Zoomed-in view of the phase-extended map from experimental phases. The final model, not included in the map calculation, is shown.

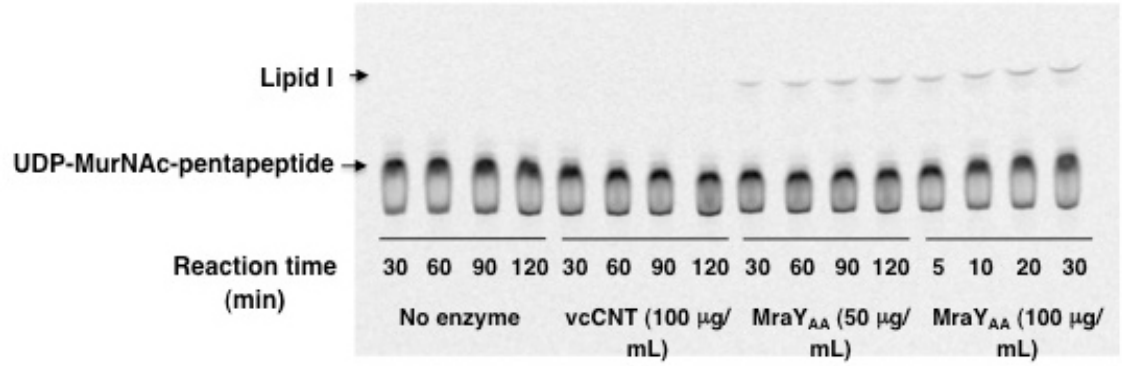


**Fig. S2**

Endogenous *E.coli* MraY does not contribute to the observed MraY$_{AA}$ activity. Two control reactions were run in parallel to those of purified MraY$_{AA}$: reactions with no enzyme added (No enzyme) and reactions containing control membrane transporter molecules (vcCNT) that were expressed and purified using the same methods as MraY$_{AA}$ (*27*). The control transporter molecules and MraY$_{AA}$ were prepared in parallel.

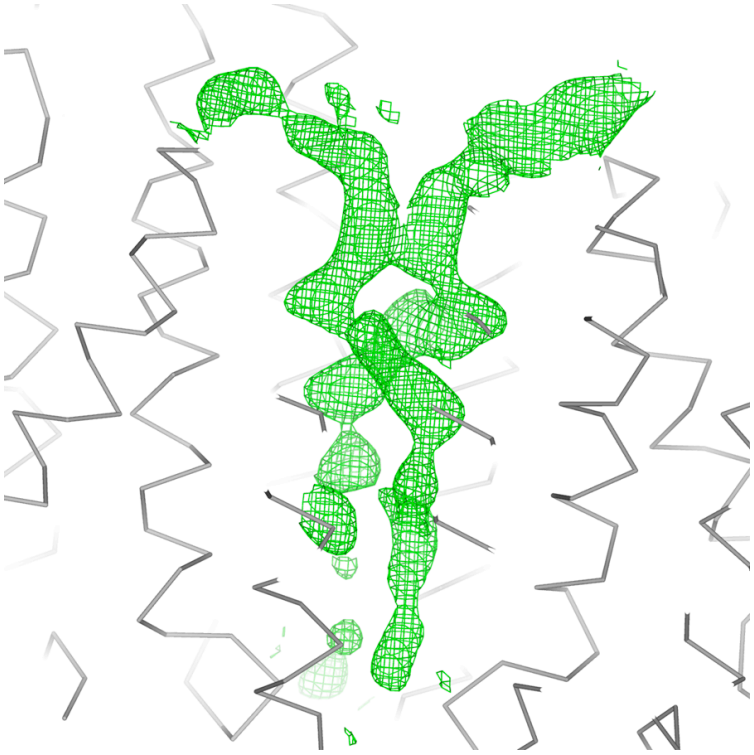

**Fig. S3**

Electron density at the dimer interface. (**A**) A $2F_O$-$F_C$ OMIT map (green) calculated with the final model phases is shown in cyan mesh contoured at 1.2σ. The protein model is shown as Cα representation and colored gray.

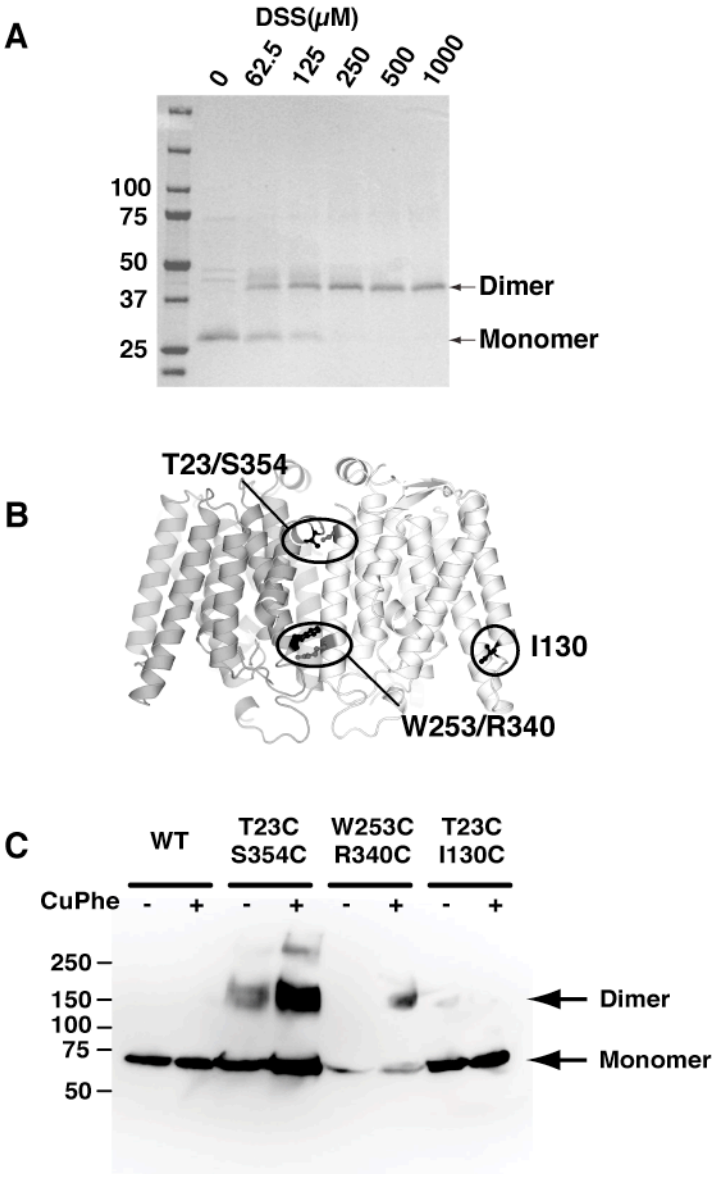


**Fig. S4**

Stoichiometry of $MraY_{AA}$. (A) Coomassie-stained SDS-PAGE analysis of cross-linking. Purified $MraY_{AA}$ in detergent micelles was treated with increasing concentrations of disuccinimidyl suberate (DSS) as indicated above the lanes. (B) Dimer interface with the amino acid residues chosen for cysteine mutations indicated with red circles. (C) Western blot analysis of cross-linking. Cell membranes containing maltose-binding protein (MBP)-fused $MraY_{AA}$, MBP-$MraY_{AA}$ (23C/354C), MBP-$MraY_{AA}$ (253C/340C), and the control MBP-$MraY_{AA}$(23C/130C) were treated with and without 200 μM copper phenanthroline (CuPhe). Note that MBP does not contain any endogenous cysteines. Molecular weight markers are indicated on the left in (**A**) and (**C**). All the cross-linking studies were performed at RT and at least three times independently.

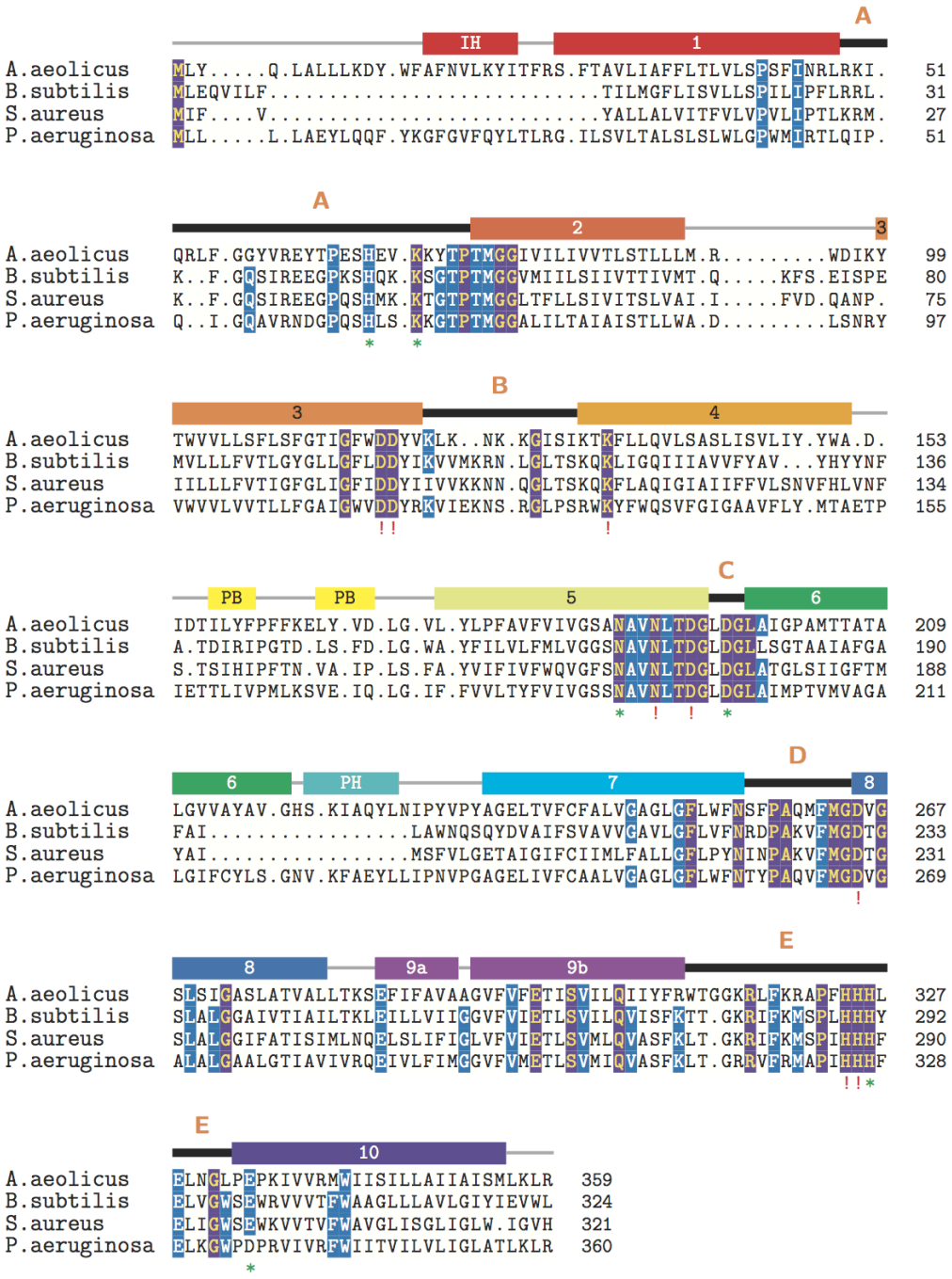


**Fig. S5**

Sequence alignment. Highly conserved positions across the MraY family are highlighted purple (100% identity) and blue (>70% identity) based on 28 MraY orthologues. Secondary structures are shown above the sequence with the same color-coding as Fig. 2. The residues with red exclamation points are essential amino acids for MraY function since mutations at these positions kill bacteria while mutations of the residues with green asterisks lower enzyme activity significantly (*16*). The species that were used for the

sequence alignment are: *Aquifex Aeolicus* (GI:15605650), *Rickettsia prowazekii* (386082453)*, Pseudomonas aeruginosa* (10719754), *Yersinia pestis* (115346359), *Bacillus anthracis* (227813177)*, Escherichia coli* (332341419), *Bordetella pertussis* (33564031), *Shigella dysenteriae* (82775494), *Bacillus subtilis* (40163)*, Aggregatibacter actinomycetemcomitans* (261867477), *Haemophilus influenzae* (68249684), *Streptococcus pneumoniae* (379070587), *Clostridium acetobutylicum* (15025117), *Staphylococcus aureus* (384861776), *Neisseria meningitidis* (254805550), *Acinetobacter baumannii* (407189484), *Neisseria gonorrhoeae* (59718768), *Streptococcus pyogenes* (383494372), *Enterococcus hirae* (3122385), *Borrelia burgdorferi* (1165287), *Helicobacter pylori* (385220721), *Chlamydia trachomatis* (237803187), *Porphyromonas gingivalis* (334147487), *Enterococcus faecalis* (2149904), *Campylobacter jejuni* (112359797), *Mycobacterium tuberculosis* (494700591), *Synechocystis sp - PCC 6803*(1006612), *Mycobacterium leprae* (130092981).

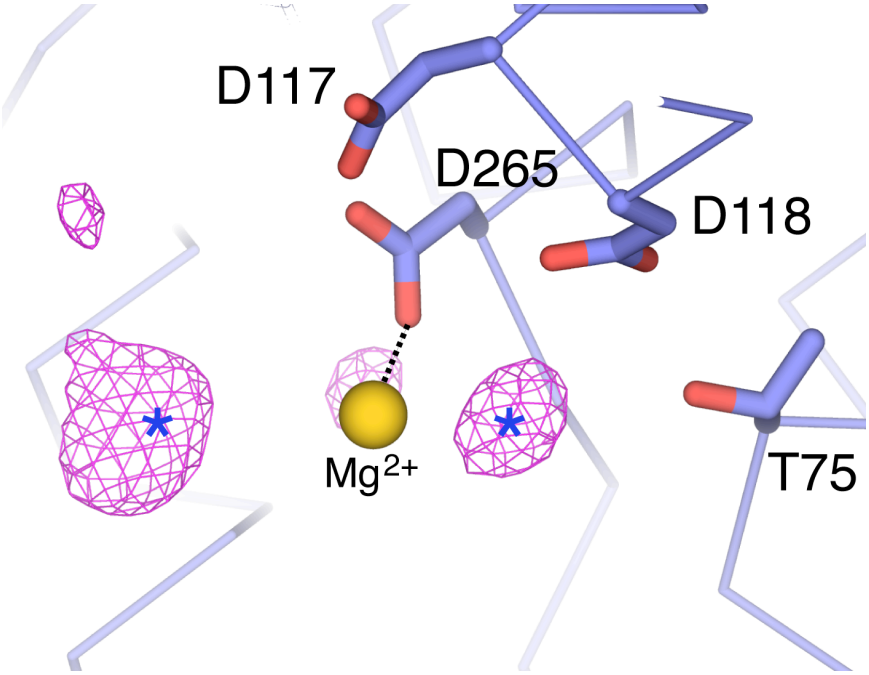


**Fig. S6**

$Mg^{2+}$ coordination. An $F_O$-$F_C$ OMIT map shows that there are two density peaks (marked with blue asterisks) that can participate in coordinating the $Mg^{2+}$ ion in the active site of $MraY_{AA}$. The map was calculated using the model phases and contoured at 3σ.

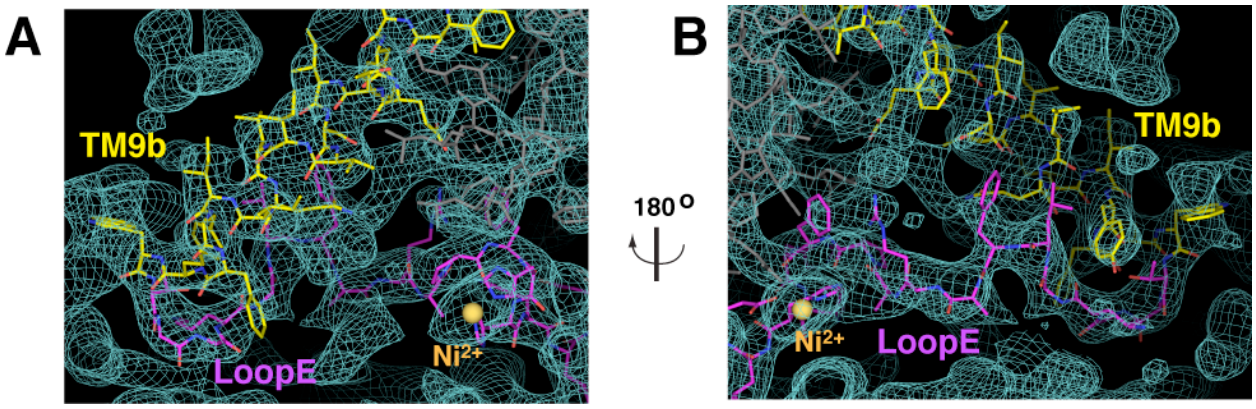


**Fig. S7**

Zoomed-in view of the TM9b/loop E region of the electron density map from experimental phases. The phase-extended and non-crystallographic two-fold averaged electron density map calculated from the 3.9 Å Se-SAD phases and the amplitudes of the 3.3-Å native data (the same map as fig. S1B). The amplitudes of the native data were subjected to anisotropic scaling prior to phase extension. The final model, not included in the map calculation, is shown with the following color scheme: TM9b (yellow), loop E (magenta), and the rest of the protein (gray).

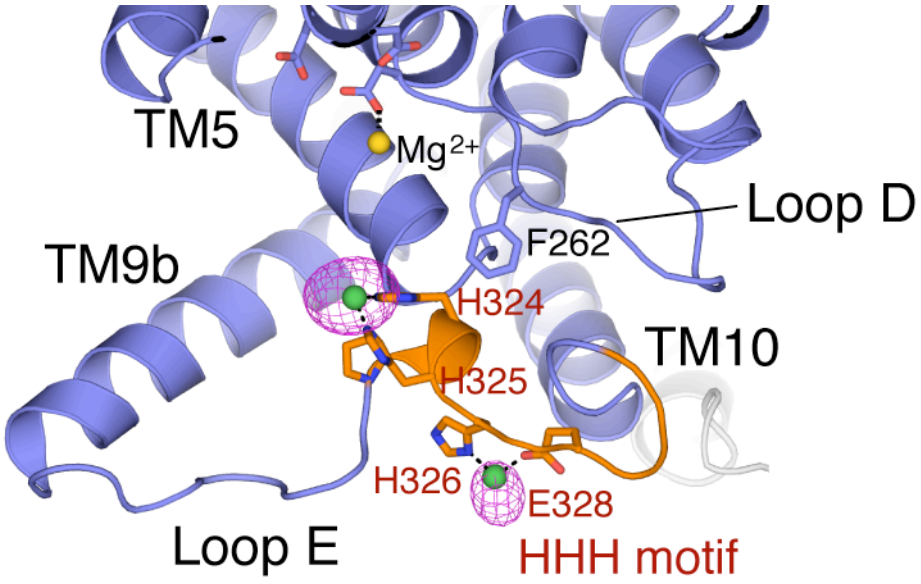


**Fig. S8**

Zoomed-in view of TM9b, loop E (the HHH motif). The structure is rotated 90$^{O}$ toward the reader relative to Fig. 3B. The HHH motif is colored orange and the side-chains of the conserved amino acid residues within the motif are shown as sticks. It appears that the loop E structure is maintained by interactions of this HHH motif with TM5 and loop D, particularly the conserved Phe$^{262}$ of loop D. The green spheres are $Ni^{2+}$, and their interactions with conserved residues are shown as dotted lines. An anomalous difference Fourier map was calculated from 30 Å - 3.3 Å from data collected at a wavelength of 0.975 Å on a native crystal grown in the presence of $Mg^{2+}$ and $Ni^{2+}$ using the model phases. Since $Mg^{2+}$ is silent (~0.06e) and $Ni^{2+}$ is strong (~1.9e) in terms of anomalous scattering power at 0.975 Å, the ions on HHH motif must be $Ni^{2+}$. The anomalous difference peaks, contoured at 5σ, are shown in magenta mesh.

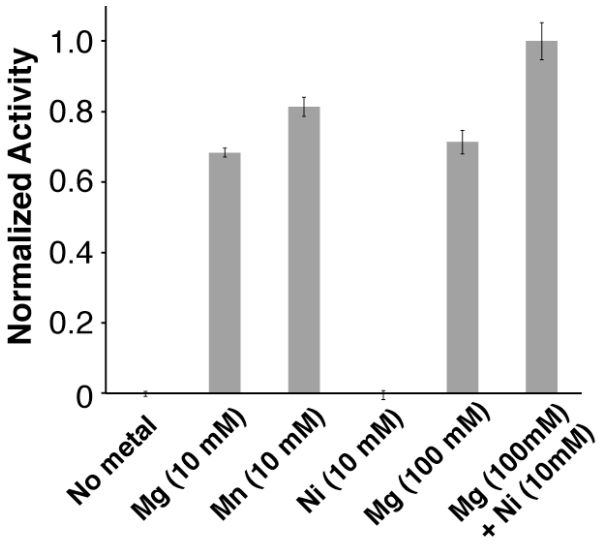


**Fig. S9**

Divalent metal dependence of $MraY_{AA}$ (n = 3, SD). The TLC-based translocase assay was performed as described in Materials and Methods.

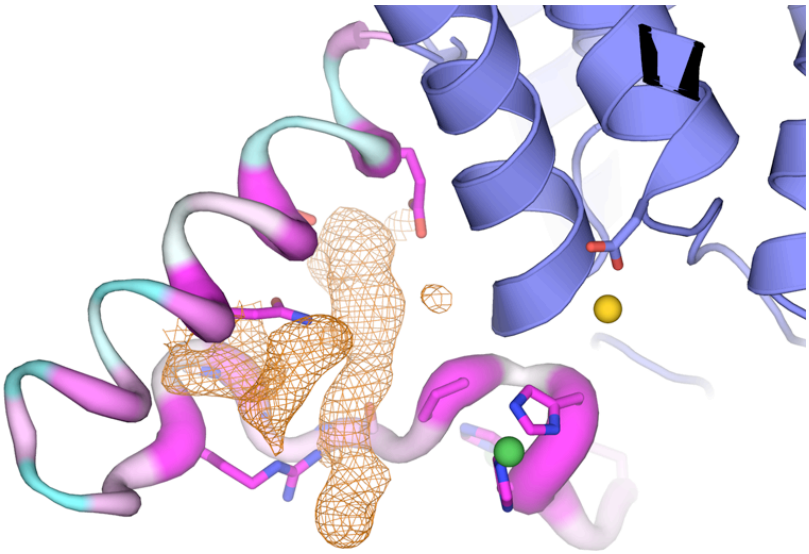

**Fig. S10**

Zoomed-in view of TM9b/loop E. TM9b/loop E is shown in sausage representation with the thicker region more conserved (magenta) and the thinner region less conserved (cyan). $Mg^{2+}$ and $Ni^{2+}$ are shown as yellow and green spheres, respectively. Fo-Fc OMIT electron density is shown in brown mesh and contoured at 2.1σ. The figure is identical to **Fig. 4A** except for the electron density.

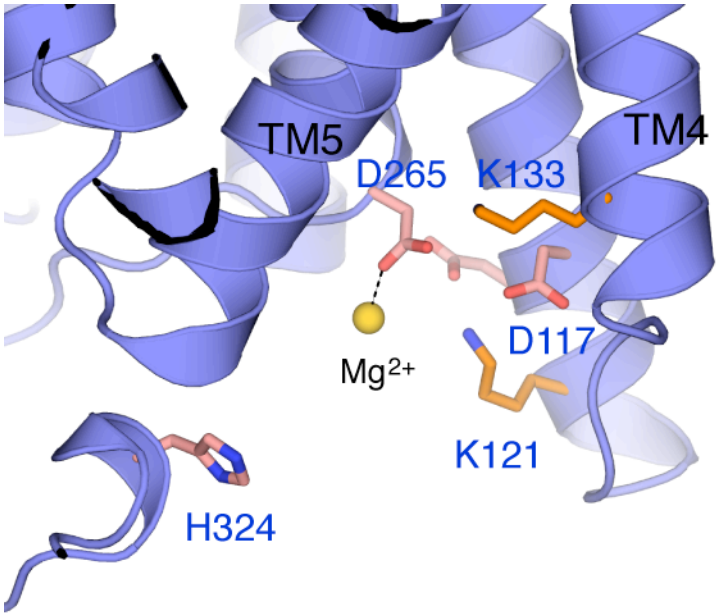


**Fig. S11**
The location of D117 within the active site. $Mg^{2+}$ is shown as a yellow sphere.

| **Data collection** | Native | SeMet | $Mn^{2+}$-co-crystal | $Mn^{2+}$-soak |
|---|---|---|---|---|
| Space group | $P2_12_12_1$ | $P2_12_12_1$ | $C222_1$ | $P2_12_12_1$ |
| Wavelength (Å) | 0.9753 | 0.9792 | 1.50 | 1.55 |
| Cell dimensions | | | | |
| *a, b, c* (Å) | 95.80, 101.49, 138.31 | 96.20, 101.55, 138.86 | 97.34,100.50, 141.68 | 97.28, 100.19, 141.12 |
| α, β, γ (°) | 90, 90, 90 | 90, 90, 90 | 90,90,90 | 90,90,90 |
| Resolution (Å) | 49.08 – 3.3 (3.36 – 3.3) | 80.00 – 3.86 (3.93 – 3.86) | 50.00 – 5.20 (5.29 – 5.20) | 50.00 – 5.70 (5.80 – 6.70) |
| $R_{sym}$ (%) | 7.1 (46.7) | 9.0 (58.0) | 4.5 (64.5) | 6.7 (67.3) |
| I/σI | 35.98 (1.97) | 31.10 (2.11) | 59.2 (3.8) | 56.12 (3.16) |
| Completeness (%) | 99.5 (97.3) | 96.0 (90.0) | 99.7 (100) | 99.6 (100) |
| Redundancy | 6.5 (3.6) | 10.8 (7.6) | 13.6 (13.2) | 10.9 (10.4) |
| **SAD Phasing** | | | | |
| Figure of Merit | | 0.32 (80 – 3.9 Å) | | |
| **Refinement** | | | | |
| Resolution (Å) | 26.7 – 3.3 (3.42 –3.30) | | | |
| Completeness (%)* | 93.76 (60.0) | | | |
| No. of reflections | 19537 | | | |
| $R_{work}/R_{free}$ | 22.3/26.5 | | | |
| **Ramachandran (%)** | | | | |
| Favored | 97.7 | | | |
| Outliers | 0.0 | | | |
| **R.m.s.d** | | | | |
| Bond lengths (Å) | 0.009 | | | |
| Bond angles (°) | 1.2 | | | |

**Table S1**. Data collection, phasing and refinement statistics.
$R_{sym} = \Sigma \mid Ii - < Ii > \mid / \Sigma Ii$, where $< Ii >$ is the average intensity of symmetry-equivalent reflections. $R_{work} = \Sigma \mid Fo - Fc \mid / \Sigma \mid Fo \mid$, where Fo and Fc are the observed and calculated structure factors, respectively. $R_{free}$ = R-factor calculated using a subset (~5%) of reflection data chosen randomly and omitted throughout refinement. The figure of merit = $|F(hkl)_{best}|/|F(hkl)|$ and was calculated using Phaser before density modification. *The data treated with ellipsoidal truncation were used for refinement (*23*).

| Resolution (Å) | Completeness | $CC_{1/2}$ |
|---|---|---|
| 49.25 - 7.11 | 0.985 | 0.988 |
| 7.11 - 5.65 | 1 | 0.997 |
| 5.65 - 4.94 | 1 | 0.997 |
| 4.94 - 4.47 | 1 | 0.998 |
| 4.47 - 4.15 | 1 | 0.996 |
| 4.15 - 3.91 | 1 | 0.992 |
| 3.91 - 3.71 | 0.996 | 0.98 |
| 3.71 - 3.55 | 0.969 | 0.955 |
| 3.55 - 3.42 | 0.811 | 0.876 |
| 3.42 - 3.30 | 0.603 | 0.728 |

**Table S2**. Completeness and $CC_{1/2}$ of the native data

**References and Notes**


1. M. Winn, R. J. Goss, K. Kimura, T. D. Bugg, Antimicrobial nucleoside antibiotics targeting cell wall assembly: Recent advances in structure-function studies and nucleoside biosynthesis. *Nat. Prod. Rep.* **27**, 279–304 (2010). doi:10.1039/b816215h Medline

2. T. D. Bugg, D. Braddick, C. G. Dowson, D. I. Roper, Bacterial cell wall assembly: Still an attractive antibacterial target. *Trends Biotechnol.* **29**, 167–173 (2011). doi:10.1016/j.tibtech.2010.12.006 Medline

3. A. Bouhss, A. E. Trunkfield, T. D. Bugg, D. Mengin-Lecreulx, The biosynthesis of peptidoglycan lipid-linked intermediates. *FEMS Microbiol. Rev.* **32**, 208–233 (2008). doi:10.1111/j.1574-6976.2007.00089.x Medline

4. D. S. Boyle, W. D. Donachie, mraY is an essential gene for cell growth in *Escherichia coli*. *J. Bacteriol.* **180**, 6429–6432 (1998). Medline

5. S. Mendel, J. M. Holbourn, J. A. Schouten, T. D. Bugg, Interaction of the transmembrane domain of lysis protein E from bacteriophage phiX174 with bacterial translocase MraY and peptidyl-prolyl isomerase SlyD. *Microbiology* **152**, 2959–2967 (2006). doi:10.1099/mic.0.28776-0 Medline

6. S. Tanaka, W. M. Clemons, Jr., Minimal requirements for inhibition of MraY by lysis protein E from bacteriophage ΦX174. *Mol. Microbiol.* **85**, 975–985 (2012). doi:10.1111/j.1365-2958.2012.08153.x Medline

7. T. Koga, T. Fukuoka, N. Doi, T. Harasaki, H. Inoue, H. Hotoda, M. Kakuta, Y. Muramatsu, N. Yamamura, M. Hoshi, T. Hirota, Activity of capuramycin analogues against *Mycobacterium tuberculosis*, *Mycobacterium avium* and *Mycobacterium intracellulare* in vitro and in vivo. *J. Antimicrob. Chemother.* **54**, 755–760 (2004). doi:10.1093/jac/dkh417 Medline

8. N. Auberger, R. Frlan, B. Al-Dabbagh, A. Bouhss, M. Crouvoisier, C. Gravier-Pelletier, Y. Le Merrer, Synthesis and biological evaluation of potential new inhibitors of the bacterial transferase MraY with a β-ketophosphonate structure. *Org. Biomol. Chem.* **9**, 8301–8312 (2011). doi:10.1039/c1ob06124k Medline

9. T. D. Bugg, A. J. Lloyd, D. I. Roper, Phospho-MurNAc-pentapeptide translocase (MraY) as a target for antibacterial agents and antibacterial proteins. *Infect. Disord. Drug Targets* **6**, 85–106 (2006). doi:10.2174/187152606784112128 Medline

10. C. Dini, Y. Mra, MraY inhibitors as novel antibacterial agents. *Curr. Top. Med. Chem.* **5**, 1221–1236 (2005). doi:10.2174/156802605774463042 Medline

11. A. B. Shapiro, H. Jahić, N. Gao, L. Hajec, O. Rivin, A high-throughput, homogeneous, fluorescence resonance energy transfer-based assay for phospho-N-acetylmuramoyl-pentapeptide translocase (MraY). *J. Biomol. Screen.* **17**, 662–672 (2012). doi:10.1177/1087057112436885 Medline

12. M. A. Lehrman, A family of UDP-GlcNAc/MurNAc: Polyisoprenol-P GlcNAc/MurNAc-1-P transferases. *Glycobiology* **4**, 768–771 (1994). doi:10.1093/glycob/4.6.768 Medline

13. A. Bouhss, M. Crouvoisier, D. Blanot, D. Mengin-Lecreulx, Purification and characterization of the bacterial MraY translocase catalyzing the first membrane step of peptidoglycan biosynthesis. *J. Biol. Chem.* **279**, 29974–29980 (2004). doi:10.1074/jbc.M314165200 Medline

14. A. Bouhss, D. Mengin-Lecreulx, D. Le Beller, J. Van Heijenoort, Topological analysis of the MraY protein catalysing the first membrane step of peptidoglycan synthesis. *Mol. Microbiol.* **34**, 576–585 (1999). doi:10.1046/j.1365-2958.1999.01623.x Medline

15. C. L. White, A. Kitich, J. W. Gober, Positioning cell wall synthetic complexes by the bacterial morphogenetic proteins MreB and MreD. *Mol. Microbiol.* **76**, 616–633 (2010). doi:10.1111/j.1365-2958.2010.07108.x Medline

16. B. Al-Dabbagh, X. Henry, M. El Ghachi, G. Auger, D. Blanot, C. Parquet, D. Mengin-Lecreulx, A. Bouhss, Active site mapping of MraY, a member of the polyprenyl-phosphate N-acetylhexosamine 1-phosphate transferase superfamily, catalyzing the first membrane step of peptidoglycan biosynthesis. *Biochemistry* **47**, 8919–8928 (2008). doi:10.1021/bi8006274 Medline

17. A. J. Lloyd, P. E. Brandish, A. M. Gilbey, T. D. Bugg, Phospho-N-acetyl-muramyl-pentapeptide translocase from *Escherichia coli*: Catalytic role of conserved aspartic acid residues. *J. Bacteriol.* **186**, 1747–1757 (2004). doi:10.1128/JB.186.6.1747-1757.2004 Medline

18. A. O. Amer, M. A. Valvano, Conserved amino acid residues found in a predicted cytosolic domain of the lipopolysaccharide biosynthetic protein WecA are implicated in the recognition of UDP-N-acetylglucosamine. *Microbiology* **147**, 3015–3025 (2001). Medline

19. M. S. Anderson, S. S. Eveland, N. P. Price, Conserved cytoplasmic motifs that distinguish sub-groups of the polyprenol phosphate:N-acetylhexosamine-1-phosphate transferase family. *FEMS Microbiol. Lett.* **191**, 169–175 (2000). doi:10.1111/j.1574-6968.2000.tb09335.x Medline

20. B. G. Fox, P. G. Blommel, Autoinduction of protein expression. *Curr. Protoc. Protein Sci.* chap. 5, unit 5.23 (April 2009) (10.1002/0471140864.ps0523s56).

21. G. M. Sheldrick, A short history of SHELX. *Acta Crystallogr. A* **64**, 112–122 (2008). doi:10.1107/S0108767307043930 Medline

22. P. D. Adams, P. V. Afonine, G. Bunkóczi, V. B. Chen, I. W. Davis, N. Echols, J. J. Headd, L. W. Hung, G. J. Kapral, R. W. Grosse-Kunstleve, A. J. McCoy, N. W. Moriarty, R. Oeffner, R. J. Read, D. C. Richardson, J. S. Richardson, T. C. Terwilliger, P. H. Zwart, PHENIX: A comprehensive Python-based system for macromolecular structure solution. *Acta Crystallogr. D Biol. Crystallogr.* **66**, 213–221 (2010). doi:10.1107/S0907444909052925 Medline

23. M. Strong, M. R. Sawaya, S. Wang, M. Phillips, D. Cascio, D. Eisenberg, Toward the structural genomics of complexes: Crystal structure of a PE/PPE protein complex from Mycobacterium tuberculosis. *Proc. Natl. Acad. Sci. U.S.A.* **103**, 8060–8065 (2006). doi:10.1073/pnas.0602606103 Medline

24. M. Kurosu, K. Li, D. C. Crick, Concise synthesis of capuramycin. *Org. Lett.* **11**, 2393–2396 (2009). doi:10.1021/ol900458w Medline

25. T. B. Clarke, F. Kawai, S. Y. Park, J. R. Tame, C. G. Dowson, D. I. Roper, Mutational analysis of the substrate specificity of *Escherichia coli* penicillin binding protein 4. *Biochemistry* **48**, 2675–2683 (2009). doi:10.1021/bi801993x Medline

26. A. J. Lloyd, A. M. Gilbey, A. M. Blewett, G. De Pascale, A. El Zoeiby, R. C. Levesque, A. C. Catherwood, A. Tomasz, T. D. Bugg, D. I. Roper, C. G. Dowson, Characterization of tRNA-dependent peptide bond formation by MurM in the synthesis of *Streptococcus pneumoniae* peptidoglycan. *J. Biol. Chem.* **283**, 6402–6417 (2008). doi:10.1074/jbc.M708105200 Medline

27. Z. L. Johnson, C. G. Cheong, S. Y. Lee, Crystal structure of a concentrative nucleoside transporter from *Vibrio cholerae* at 2.4 Å. *Nature* **483**, 489–493 (2012). doi:10.1038/nature10882 Medline